Raman Spectroscopy: Analysis of Graphene, Carbon Nanotubes and Transition Metal Dichalcogenides

Szymon Bartuś

Abstract

The following literature review highlights the use of Raman spectroscopy for analysis of three classes of nanomaterials: carbon nanotubes, graphene and transition metal dichalcogenides (TMDs). Analysis of Raman spectra can provide valuable structural information about the material as well as experimental verification of theoretical predictions. The technique is already widely used in carbon nanotube and graphene research. The new field of thin transition metal dichalcogenide layers is also expected to benefit from it.

Table of contents

1. Introduction

Raman effect – the inelastic scattering of photons by matter – has been used for several decades in a variety of analytical methods. The discovery of this phenomenon by Chandrasekhara Venkata Raman in 1928[1] immediately initiated a large interest, resulting in 58 papers on Raman scattering in the same year[2]. With the introduction of commercial infrared (IR) spectrometers in 1940s, the interest in Raman spectroscopy diminished but after invention of lasers in early 1960s it revived again[2]. Further developments in Raman spectrometer design included the use of Fourier transform (FT) and charge-coupled device (CCD) detectors[3]. Many alterations to the "standard" Raman spectroscopy have been developed. For instance, tuning the excitation light frequency so that it matches an electronic transition in the analyzed material enhances the intensity of the Raman scattering[4], what is known as resonance Raman scattering. Another method to increase the intensity is the surface-enhanced Raman spectroscopy (SERS), where molecules of the analyte are adsorbed on solid surface[5]. Raman spectra of very small samples or solid surface details can be recorded using Raman microscopy[6]. In Raman imaging, a special type of spectrometer scanning a solid surface can construct an image of that surface at a given wavelength[7]. The spectra can also be resolved in time to analyze transient species[8]. Not only the intensity of the scattered light can be analyzed – a relatively new research area called Raman optical activity (ROA) is concerned with analyzing the polarization of light scattered from optically active compounds[4]. Today's uses of Raman spectroscopy are extremely diverse and include areas like forensics[4], archeology[9] and industrial process control[10].

Currently, Raman spectroscopy is also being used to analyze several major classes of nanomaterials, giving important information about their atomic structure as well as electronic and vibrational behavior. In the following report, the use of Raman spectroscopy is discussed in context of three families of nanomaterials: carbon nanotubes[11], graphene[12] and transition metal dichalcogenides (TMDs)[13]. For each material, the most important spectral features are highlighted, together with their origin and information which they convey about the sample.

2. About C. V. Raman

Chandrasekhara Venkata Raman (1888 - 1970), discoverer of the effect now known as Raman scattering, was an outstanding researcher and one of the founders of modern science in India. In 1930, he was awarded Nobel Prize in Physics for his findings. Two interesting biographical articles were written by Jayaraman *et al.* (Raman's coworkers) in 1988[14] and by Miller *et al.* in 1989[2] and the following text is based on both.

Figure 2.1. C. V. Raman in 1930, the year he was awarded the Nobel Prize. Image taken from[2].

Chandrasekhara Venkataraman (later, he spelled his name as two words) was born as the second of eight children in a modest Indian family. His mother was daughter of a Sanskrit scholar and his father, although coming from a landholder family, graduated from a physical sciences course and taught mathematics and physics (in high school and later at college in Vishiakapantam). Raman's abilities showed up early – he enrolled at university (Presidency College in Madras) at the age of 11 and he graduated with a BA degree getting top marks. He was advised to continue his education in England, but after a health examination by Chief Surgeon of Madras, he was declared unfit for English climate, so instead he started a master degree again at Presidency College. While performing a routine optics experiment in his class, Raman found that when light is reflected from a prism at an oblique angle, diffraction pattern can be observed. He submitted his findings to *The Philosophical Magazine*[15], which was followed a year later by a communication describing his new way of measuring surface tension[16]. These papers were written solely by Raman when he was still a teenager. He graduated with an MA degree at the age of 18, again with top honors. Perhaps because science careers were closed for Indians who weren't educated abroad, Raman then entered civil service in the Finance Department in Calcutta. He married a 13.5-year old girl named Lokasundari Ammal and the couple moved to Calcutta. Soon after moving, Raman noticed a sign *Indian Association for Cultivation of Science* on the same street where his workplace was. The institution had been founded around 30 years earlier to both educate and pursue research, but in 1907 there

were no research activities – the organization's lecture halls were just used for science courses for students. On the same day, Raman knocked their door and was admitted by Ashutosh Day, who soon became his devoted assistant. After asking whether he could conduct research in spare time, he was warmly welcomed and was immediately given access to the (then idle) laboratories. In the next ten years, Raman and Dey published 30 papers about acoustics and optics, in journals including *Nature* and *Physical Review*. At that time, Raman was only working part time (before and after his working hours and during the weekend). Meanwhile, Asutosh Mookerjee, a vice-chancellor at Univesity College of Science at Calcutta, had a vision of building a first class institution and saw Raman as an ideal candidate for the physics professorship. Notable staff already working at University College included M. Saha (known for Saha ionization equation) and S. N. Bose (known for Bose-Einstein statistics). Raman accepted the offer, despite five times lower salary than from his civil service work. In 1921, Raman departed for his first journey abroad to attend the *Congress of Universities of the British Empire* in Oxford, England, where he met famous British physicists including W. Bragg, J. J. Thomson and E. Rutherford. At that time, he got intensely fascinated by scattering of light. In fact, he obtained his first publishable result on the ship during the journey back. Lord Kelvin had stated that sea is blue just because of the reflection of blue sky. Raman simply directed a Nicol prism at a Brewster angle at the water surface, absorbing this way all the reflected light. The remaining light was still blue, a proof that the color must come from scattering instead. This result was published in *Nature* with the address given as "Bombay Harbour".[17] Back in his university labs in Calcutta, Raman started an extensive series of experiments devoted to light scattering. In 1923, Raman and his student observed that when a beam of sunlight was passed through a filter, scattered in a very pure water and then passed through a complementary filter, a faint light can be observed. This light of a different wavelength was initially thought to be a kind of fluorescence but careful purification of water didn't change anything. Later experiments also showed that many other pure liquids as well as vapors exhibit similar scattering. These observations were published in early 1928 in *Nature*[1], followed soon by another article after using mercury lamp as the light source and a small spectroscope to analyze the scattered light. In his third paper[18], submitted only 36 days after the first one, Raman already notices that the spacing between the exciting light and inelastically scattered light peaks is "of the same order of magnitude as the frequency of the molecular infra-red absorption line". The discovery was immediately acclaimed in the scientific community and the 1930 Nobel Prize in Physics was awarded to Raman *for his work on the scattering of light and for the discovery of the effect named after him*[19]. He was the first Asian Nobel laureate in science. Around that time he also got interested in the properties of diamond, including naturally it's Raman spectrum. In 1933 Raman left Calcutta to become the director of the Indian Institute of Science, a research organization founded by famous industrialist J. Tata in 1909. After analysis of some diamond spectra, he went into

the study of lattice dynamics, where he spurred controversy by criticizing theories of Born, Debye and other researchers. Similarly, he tried to explain some optical properties of diamonds by a hypothesis that diamond can exist in two forms: with tetrahedral and octahedral symmetry (later, it was shown that these properties originate from nitrogen impurities). Regardless of that, Raman made some genuine contributions at that time, including theoretical descriptions of diffraction of visible light on sound waves in fluids and of phase transitions of quartz. In 1948, he retired from the Indian Institute of Science to realize the vision of his own institution – the Raman Research Institute. After painstaking fundraising efforts, the new organization opened in 1949, where Raman worked until his death in 1970. The institute still exists today and conducts research in several areas of physics (website: www.rri.res.in).

Chandrasekhara Venkata Raman left behid a huge legacy – he authored over 450 papers, trained numerous students, and put new life in the institutions where he worked. He established the Indian Academy of Sciences, with its annual conferences and a journal. At the time of his death, his recognition in India was so large that when the prime minister Indira Ghandi heard the sad news, he called Raman's wife to ask whether she needs any financial support from the government.

3. Raman scattering – basic theory

3.1. Introduction

Raman scattering (Raman effect) occurs when the light scattered from the sample is scattered inelastically – the scattered light has a different wavelength than the incident light. When a sample, which can be gaseous, liquid or solid - is irradiated with light of frequency ν_0 (today always a laser light), that light will be scattered in all directions. Most of the scattering will occur without change in frequency (elastically) in what is known as *Rayleigh scattering*, however a small fraction of the scattered light will have a frequency $\nu_0 \pm \nu_m$ (**Figure 3.1**)[20]. Raman scattering is very weak – only around 10^{-5} of the incident beam intensity is scattered in this fashion[20].

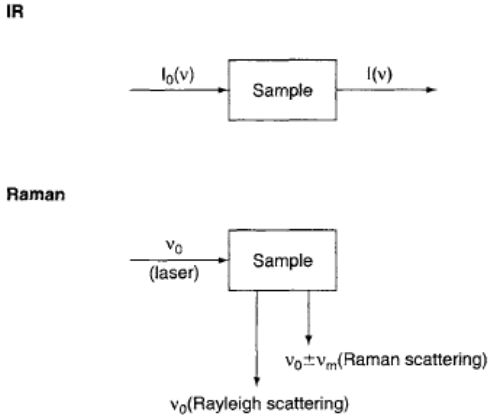

Figure 3.1. Rayleigh and Raman scattering on the analyzed sample. An IR spectroscopy setup is shown for comparison. Image taken from[20].

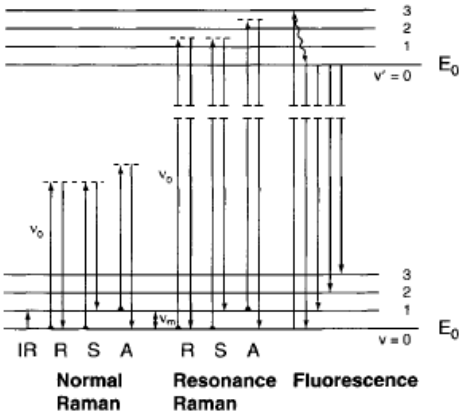

Figure 3.2. Molecular energy level diagram for IR absorption, normal (vibrational) Raman scattering, resonance Raman scattering and fluorescence. E_n denotes electronic levels and v denotes vibrational levels. Image taken from[20].

The gain or loss of energy corresponds to a transition in the sample - either rotational, vibrational or electronic. The energy diagram showing vibrational Raman transitions in a molecule is shown in **Figure 3.2.** The energy levels denoted with dashed lines are "virtual" states and don't have to correspond to "real" states (eigenstates) of the system[21]. Because of this, the exciting light can have in principle any frequency. Vast majority of the uses of Raman spectroscopy is concerned with vibrational transitions, but in case of gases, one may observe rotational transitions in the Raman spectra and, for instance in case of lanthanide ions[22], electronic transitions. This way, in Raman spectroscopy, the shift from the excitation frequency is measured (called simply "Raman shift") – an example of a vibration Raman spectrum (spectrum of CCl_4) is shown in **Figure 3.3**. The $\nu_0-\nu_m$ and $\nu_0+\nu_m$ lines are customarily called *Stokes lines* and *anti-Stokes lines,* respectively. Because the vibrational ground state is much more populated than the excited state at room temperature, Stokes lines are

stronger in the spectrum and since they both give the same information, it's usual to include only Stokes lines in the spectrum[20].

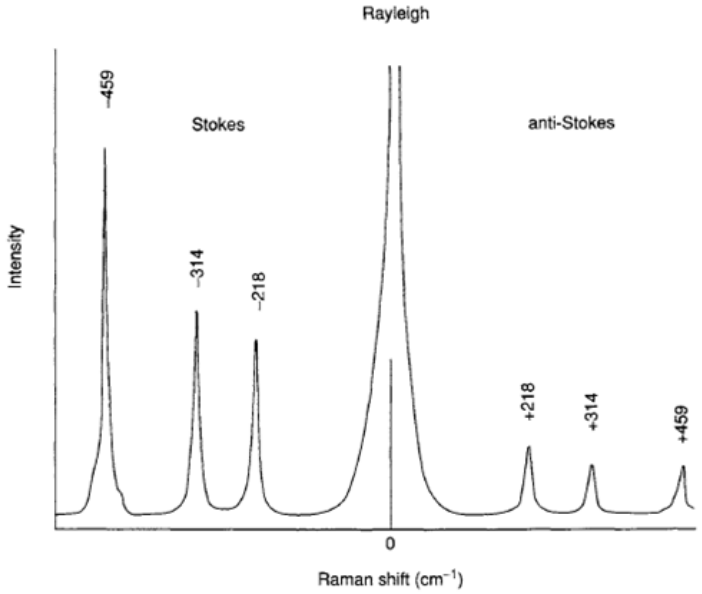

Figure 3.3. Vibrational Raman spectrum of CCl_4. Image taken from[20].

3.2. Classical description

A simple classical description, considering diatomic molecule interacting with an electromagnetic wave can explain Raman scattering[20]. Essentially the same derivation can be written for atoms in a solid[23]. The electric field strength (*E*) of the electromagnetic wave (laser) changes in time (*t*):

$$E = E_0 cos(2\pi \nu_0 t) \qquad (3.1)$$

where E_0 is the amplitude and ν_0 is the frequency. Irradiation with this light of a diatomic molecule induces an electric dipole P:

$$P = \alpha E = \alpha E_0 cos(2\pi \nu_0 t) \qquad (3.2)$$

where α is polarizability (in the direction of E). The nuclear displacement of that molecule (q) oscillates with frequency ν_m:

$$q = q_0 cos(2\pi \nu_m t) \qquad (3.3)$$

where q_0 is the amplitude of vibration. Assuming that for small displacements, α varies linearly with q, we can write:

$$\alpha = \alpha_0 + \left(\frac{\partial \alpha}{\partial q}\right)_0 q \qquad (3.4)$$

where α_0 is the polarizability at equilibrium position. After combining (3.2), (3.3) and (3.4) we obtain:

$$
\begin{aligned}
P &= \alpha E_0 cos(2\pi\nu_0 t) \\
&= \alpha_0 E_0 cos(2\pi\nu_0 t) + \left(\frac{\partial\alpha}{\partial q}\right)_0 q E_0 cos(2\pi\nu_0 t) \\
&= \alpha_0 E_0 cos(2\pi\nu_0 t) + \left(\frac{\partial\alpha}{\partial q}\right)_0 q_0 cos(2\pi\nu_m t) E_0 cos(2\pi\nu_0 t) \\
&= \alpha_0 E_0 cos(2\pi\nu_0 t) + \frac{1}{2}\left(\frac{\partial\alpha}{\partial q}\right)_0 q_0 E_0 [cos(2\pi(\nu_0+\nu_m)t) + cos(2\pi(\nu_0-\nu_m)t)]
\end{aligned}
\quad (3.5)
$$

The first term oscillates with frequency ν_0, so it corresponds to Rayleigh scattering, while the second term corresponds to Raman scattering with frequency $\nu_0+\nu_m$ (anti-Stokes) and $\nu_0-\nu_m$ (Stokes). If polarizability doesn't change with displacement, the second term becomes zero and no Raman scattering is observed. This way, we obtained an important selection rule for vibrational Raman scattering: in order to be Raman-active, the polarizability must change during the vibration mode.

3.3. Raman scattering intensity and resonance Raman scattering

The intensity of first order Raman scattering as a function of laser energy can be expressed as[24]:

$$
I(E_{laser}) = \left| \frac{A}{(E_{laser} - E_g - i\gamma_r)(E_{laser} - (E_g \pm E_q) - i\gamma_r)} \right|^2 \quad (3.6)
$$

where E_g is an electronic transition energy (eg. band gap in a semiconductor), E_q is energy of the excited vibration (in solids: phonon) and A is a constant depending on a specific system. The FWHM of each peak in the $I(E_{laser})$ dependence will be equal to γ_r, which is known as *resonance window* width. When laser energy is close to either E_g or $E_g \pm E_q$ then the denominator in (3.6) increases, giving higher scattering intensity and this is what we call *resonance* Raman scattering. This way, either the incident light, Stokes-scattered light or anti-Stokes scattered light can be in resonance. The effect of resonance is very important in nanoscale systems – the small size of the sample causes the Raman signal to be very weak[23]. To give a specific example, Jorio *et al.* measured the resonance window of a radial breathing mode (RBM) peak in an isolated single wall nanotube by varying the exciting laser energy[25]. The resonance window width was 8 meV (ca. 20 nm wavelength variation) for both Stokes and anti-Stokes scattered light and the RBM peak wasn't observed outside it. Naturally, the observation of resonance can also be used to measure the electronic transition energy, as was done here. Even a spectrum obtained at single excitation wavelength can be used to obtain the transition energy by measuring the intensities of the Stokes and anti-Stokes peaks and fitting a transition energy value to equation (3.6)[26].

3.4. Order of scattering

Raman scattering in solids can be classified depending on how many scattering events take place and how many phonons are excitied. The diagrams in **Figure 3.4.** show electron dispersion graphs (i.e. electron energy versus wavevector) for graphene with different kinds of resonance Raman scattering. The simplest case is when the excited electron creates (a1) or absorbs (a2) a single phonon and returns to the ground state. However, the excited electron can also excite a phonon and then be scattered from a defect (b1-b4) or excite 2 phonons consecutively (c1-c2). In b1-b4 and in c1-c2, the electron has energy equal to some energy level two times, what is known as *double* resonance. The intensity of second order scattering is described by formulas analogous to (3.6), with three terms in the denominator[27].

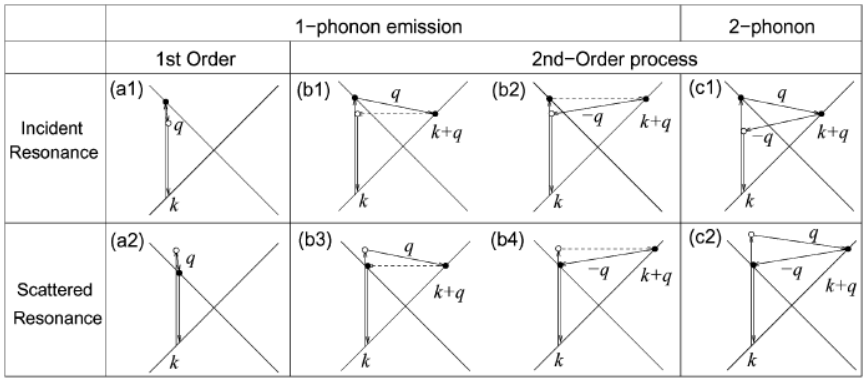

Figure 2.4. Different Raman scattering resonances with electronic levels of graphene. Taken from[28].

3.5. Selection rules

Selection rules in Raman spectroscopy are based on group theory as well as other considerations, like momentum conservation during scattering in solids. The topic of selection rules is a large one and therefore is outside the scope of this text. For a readable introduction to both molecular and solid state selection rules, see[29]. For introduction to the theory behind the selection rules which are used in Raman spectroscopy of nanocarbons, see[30]. Finally, for a book entirely about theory of Raman effect, see[31].

4. Raman spectroscopy of sp^2 nanocarbons

4.1. Overview

Carbon has been known to humanity in many forms since antiquity. Despite that, carbon-based materials are currently an important subject of research in nanoscience and nanotechnology. In 1985, a new important allotrope of that element was discovered[32]: C_{60} fullerene molecules. Widespread research of fullerenes was soon followed by an even more intense rush into carbon nanotube research after the discovery of multi-wall carbon nanotubes (MWNTs)[33] and then single-wall carbon nanotubes (SWNTs)[34,35] in early 1990s. Nanotubes turned out to have many unique mechanical, electronic, optical and other properties, which are described in several dedicated books[36,37]. Many applications of both pure nanotubes and nanotube composites have been proposed, perhaps the most spectacular being the structural material for the *space elevator* cable[38]. Finally, the isolation of monolayer graphene sheets by Novoselov *et al.* in 2004[39] led to the massive amount of interest in this material which we observe today. Despite being used as a theoretical model for a long time, graphene revealed many exciting properties and promises many useful applications, a taste of which can be found in review articles written by discoverers themselves[40,41].

Over the years, Raman spectroscopy proved to be a powerful tool to analyze carbon nanotubes and graphene[11,12,42,43]. The factors that influence Raman spectra of these materials include: strain, nanotube diameter, number of walls in the nanotube, optical transition energy, number of graphene layers and structural defects[42]. This way, important structural and electronic information can be obtained. The Raman spectra of several sp^2-hybridized carbon forms are shown in **Figure 4.1**. They contain some common features, such as the presence of G and G'-bands but, as described below, the appearance of these bands and presence of other signals are strongly influenced by the properties of the individual material sample.

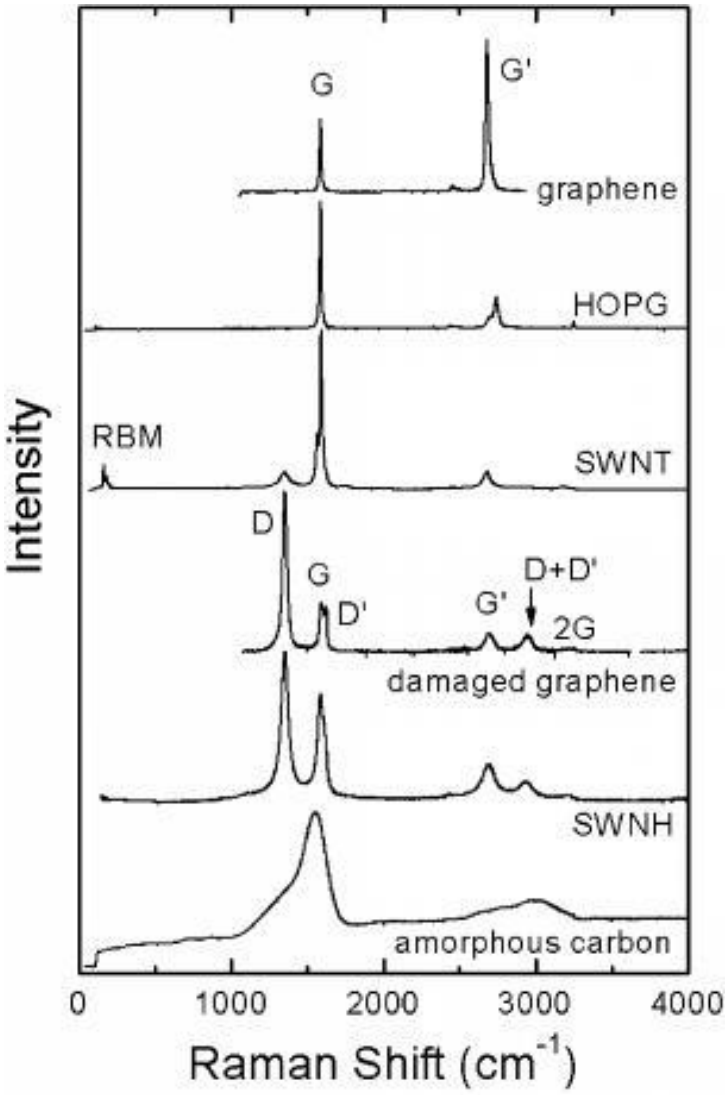

Figure 4.1. Raman spectra of monolayer graphene, highly oriented pyrolytic graphite (HOPG), single wall nanotube (SWNT), damaged graphene, single walled nanohorn and amorphous carbon. From[44].

4.2. G-band

Graphene. The G-band (where G stands for "graphite") is present in all sp^2 carbons and is caused by exciting phonons of in-plane stretching of C-C bonds. Because of their hexagonal symmetry, graphene and graphite normally exhibit a single G-band peak at around 1580 cm^{-1} [44]. It originates from two degenerate vibration modes – in-plane transverse optical (iTO) and longitudinal optical (LO)[45]. When this symmetry is broken, the modes are no longer degenerate and the G-band splits. This is the case when, for example, the graphene sheet is mechanically strained – it was shown that under a uniaxial (i.e. one dimensional) strain, the G-band splits into two peaks, with size of splitting proportional to the applied strain[46]. These two peaks, called G^+ and G^- (higher and lower frequency), correspond to the vibration modes perpendicular and parallel to the strain direction respectively[46].

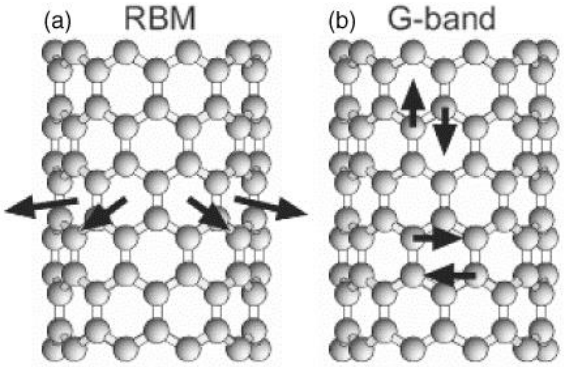

Figure 4.2. Schematic representation of the ring breathing mode (RBM) and the transverse (lower arrows) and longitudinal (upper arrows) G-band modes in carbon nanotubes. Taken from[94].

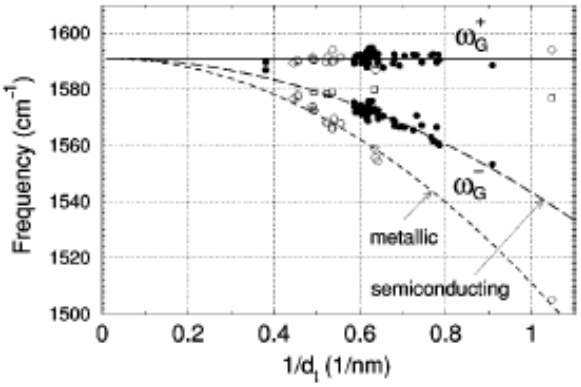

Figure 4.3. Frequency of G-band peaks for 62 measured SWNTs. The lines depict equation (6). Taken from[49].

Nanotubes. In carbon nanotubes, the G-band has a more complicated structure as the G vibrational modes consist both of vibrations along the nanotube axis (transverse) and along (or nearly along[47]) the circumference (longitudinal)[45]. They are shown schematically in **Figure 4.2**. There are three transverse and three longitudinal modes, differing in the number of vibration nodes along the tube circumference, called (after their symmetry labels) A_1, E_1 and E_2. The observation of these modes is sensitive to polarization of incident light and resonance conditions[45,48]. However, only two A_1 modes usually dominate the G-band, called again G^+ and G^- (higher and lower frequency)[45]. After comprehensive measurements of 62 isolated single wall nanotubes it was found[49] that there is a simple relation between the frequency (in cm^{-1}) of the G-band peaks and diameter of the nanotube:

$$\omega_G = 1591 + C/d_t^2 \qquad (4.1)$$

where $C_{G+} = 0$, $C_{G-}(S) = 47.7\ cm^{-1}nm^2$ and $C_{G-}(M) = 79.5\ cm^{-1}nm^2$ for semiconducting (S) and metallic nanotubes (S). The collected data is shown in **Figure 4.3**. The shape of the G^- peak is also visibly different for the metallic tubes, which was already observed earlier[50].

It is tempting to think that the G^- mode is the transverse (along the circumference) mode because it depends on the diameter and the other one doesn't[45]. However, a computational (density functional theory) study found that in metallic nanotubes it is the longitudinal mode that changes with diameter more, due to the electronic structure of the metallic tubes[51].

4.3. G'-band

As shown in **Figure 4.1**, all forms of sp^2 carbon exhibit a band in the 2500-2800 cm^{-1}, called G'-band[52]. The G'-band originates from second-order two-phonon scattering, where two phonons of opposite momentum are excited consecutively[52] (**Figure 3.4 c1, c2**). Typically, G'-bands are observed when double resonance occurs. Characteristic for the G'-band is the dependence of its frequency on the laser excitation energy, known as *dispersive* behavior. This is unusual for peaks in Raman spectra as Raman shift typically doesn't depend on excitation light energy. In both graphene and nanotubes the dispersive behavior is the direct result of double resonance with electronic energy levels in these systems[52].

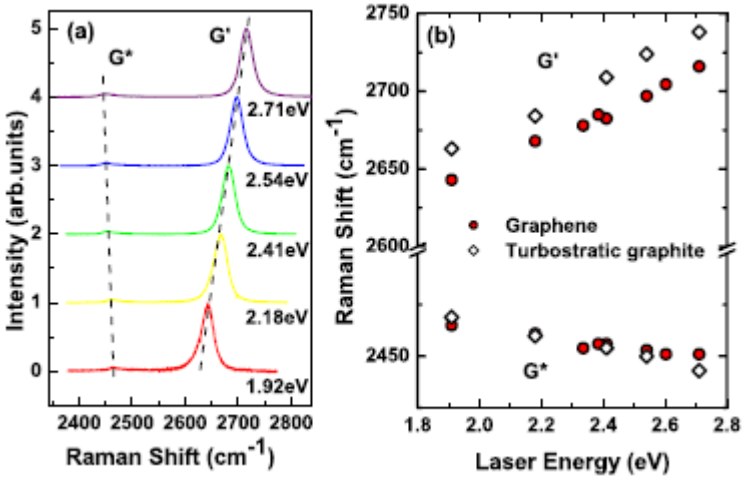

Figure 4.4. (a) Raman spectra monolayer graphene recorded with various laser excitation energies. (b) Dependence of Raman shifts of G' and G* bands on the excitation energy for monolayer graphene and turbostratic graphite[53].

Graphene. In graphene, the G'-band results from exciting two iTO (in-plane transverse optical) phonons with opposite momenta[52,53]. Mafra *et al.* have measured Raman spectra of both monolayer graphene and turbostratic graphite with excitation energies between 1.92 and 2.71 eV, shown in **Figure 4.4**[53]. The obtained G'-band frequency dependence on the laser energy was ca. 88 cm^{-1}/eV for monolayer graphene and 95 cm^{-1}/eV for turbostratic graphite. They also used the obtained frequencies of G' and G* bands[(1)] to find the relative velocities of iTO and LA (longitudinal acoustic)

[1] G* band is another band originating from two phonon scattering and observed with double resonance, but as can be seen on Figures 4.1 and 4.4 it's not prominent on the spectra.

phonons. Assuming double resonance with electronic energy levels, it can be shown that the velocity of phonons in graphene can be calculated as:

$$v_{TO} = \left(\frac{1}{2} \frac{\mathrm{d}\omega_{G'}}{\mathrm{d}\omega_l} \right) v_F$$
$$v_{LA} = \left(\frac{\mathrm{d}\omega_{G^*}}{\mathrm{d}\omega_l} - \frac{1}{2} \frac{\mathrm{d}\omega_{G'}}{\mathrm{d}\omega_l} \right) v_F \qquad (4.2)$$

where v_{TO} and v_{LA} are velocities of iTO and LA phonons, ω is the angular frequency of laser, G' or G* peaks and v_F is the Fermi velocity. The values obtained from the slopes of **Figure 4.4 (b)** were: $v_{LA} = 7.70 \cdot 10^{-3} v_F$ and $v_{TO} = 5.47 \cdot 10^{-3} v_F$ for monolayer graphene and $v_{LA} = 9.82 \cdot 10^{-3} v_F$ and $v_{TO} = 5.96 \cdot 10^{-3} v_F$ for turbostratic graphite. The results for graphene were then used to compare the experimental data with theoretically calculated phonon structures and a good agreement was obtained when $v_F = 1.00 \cdot 10^6$ m/s was used. In this way, Raman scattering helped to verify theoretical predictions of the graphene phonon structure.

An important feature of the G'-band for the graphene characterization is that its appearance changes with the number of graphene layers. Raman spectrum of a single layer graphene (**Figure 4.1**) shows a single peak in the G'-band. In case of more layers, the G'-band shape is more complicated, as shown in **Figure 4.5**. For bilayer graphene, the band is broader and is made of 4 peaks which originate from 4 different double resonances with the electronic levels, as shown in **Figure 4.6**[54,55]. For more layers, the number of peaks increases, but then the band converges into two peaks for highly oriented pyrolytic graphite (**Figure 4.5**), each of these peaks corresponding to very large number of resonances[56].

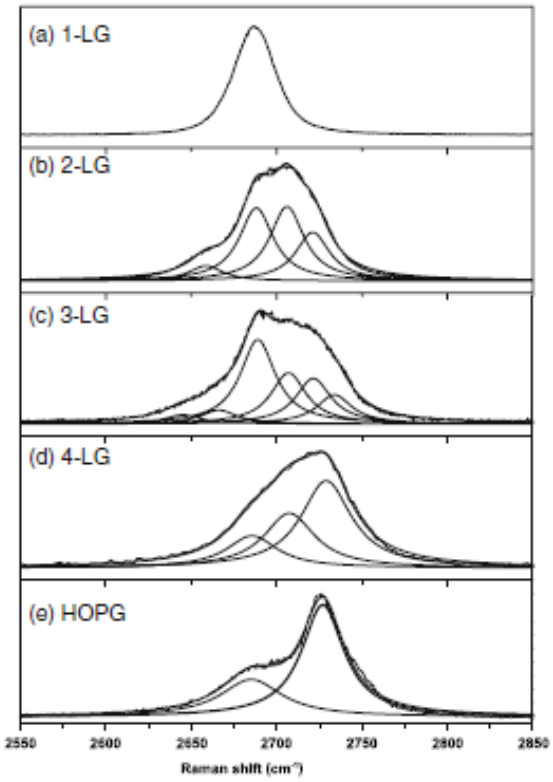

Figure 4.5. G'-band measured with 2.41 eV exciting laser for single and multi-layer graphene and for highly-oriented pyrolytic graphite (HOPG)[12]. The bands were fitted with Lorentzian peaks.

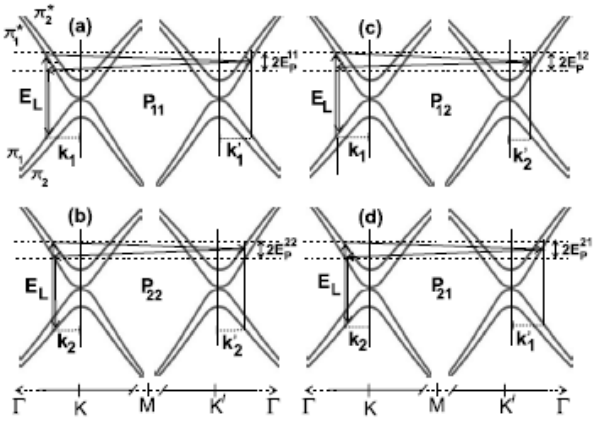

Figure 4.6. Resonances causing four peaks in the G'-band of bilayer graphene. Each graph is an electron dispersion relation (electron momentum coordinates on the horizontal axis and electron energy on the vertical axis). The vertical arrows depict photon absorption/emission while horizontal arrows depict phonon creation. Taken from[55].

The shape of G'-band is also sensitive to the stacking order – in the measurements described above the layers of graphene were stacked in AB Bernal fashion (i.e. the one present in HOPG). As opposed to HOPG, turbostratic graphite shows a single peak in the G'-band, but this peak is ca. 2 times broader and upshifted comparing to monolayer graphene[12]. Bilayer graphene with arbitrarily oriented layers also shows a single G' peak[57]. For more detailed discussion of influence of number of graphene layers and stacking order on Raman spectra, see[12].

Nanotubes. In single wall nanotubes, the dependence of G'-band frequency on laser energy also increases (approximately) linearly, however this can be only directly observed in samples containing a bundle of different nanotubes[52]. This is because each (n, m) nanotube has its own discrete electronic transition energies and so different tubes enter resonance with different laser energies[52,58]. In the linear growth there are some fluctuations as different tubes are in resonance[52,58]. In some isolated SWNTs, the G'-band consists of two overlapping peaks, as shown in **Figure 4.7**. The two peaks originate from both incident laser and scattered photon being in resonance with two different electronic transitions[11,59]. This behavior is not present in all nanotubes and it depends on the semiconducting or metallic character of the tube. For a detailed discussion and a literature review about the origin of G'-band in single wall carbon nanotubes, see[11]. A two-peak G'-band was also observed for in a chemically doped nanotubes[60].

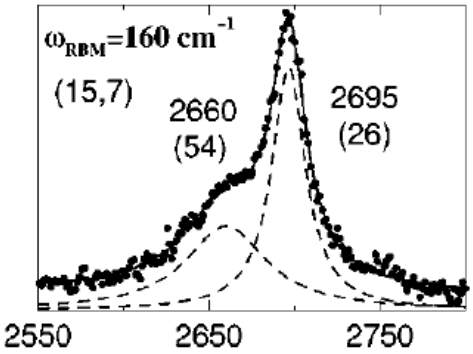

Figure 3.7. G'-band for a (15,7) semiconducting nanotube. From[59].

4.4. Radial breathing mode

Radial breathing mode (RBM) is the vibrational mode of nanotubes where the atoms are simultaneously displaced radially (**Figure 4.2**). As expected, this mode is sensitive to the tube diameter. Using classical mechanics (elasticity theory) one can derive[61] the frequency (wavenumber) of the radial breathing mode as:

$$\omega_{RBM} = \sqrt{\frac{Y}{\rho}}\frac{1}{R} = \frac{A}{d_t} \qquad (4.3)$$

where Y is Young's modulus of the graphite along the planes, ρ is density, R is tube radius, d_t is tube diameter and $A = 2(Y/\rho)^{0.5}$. It turns out that in elasticity theory $(Y/\rho)^{0.5}$ is equal to the speed of sound for the longitudinal mode, which after substituting gives A = 227 cm^{-1} nm. Note that for flat graphene plane (d_t = infinity) the frequency is zero, as it should be. Relation (7) with this value of A holds for nanotubes vertically aligned on a substrate, as was shown by Araujo *et al.* who analyzed a sample of

197 nanotubes synthesized by water-assisted chemical vapor deposition (CVD) method[62]. They noticed however that the RBM frequencies of the samples analyzed elsewhere in the literature, which were in different environments (eg. lying on a flat substrate) varied and so they used a modified equation to compensate for these environmental effects. The equation, which is derived by considering a hollow cylinder subjected to external pressure (originating from van der Waals attraction) is:

$$\omega_{RBM} = \left\{ \frac{1}{\pi c} \sqrt{\frac{Eh}{\rho h(1-\nu^2)}} \right\} \sqrt{\frac{1}{d_t^2} + \frac{6(1-\nu^2)}{Eh} \frac{K}{s_0^2}} \qquad (4.4)$$

where E is Young's modulus, h is thickness of the environment shell , v is Poisson's ratio, s_0 is equilibrium separation between the tube wall and environment and K is the van der Waals interaction strength. The curly bracket is, as above, equal to 227 cm^{-1} nm. The best fit with literature data was obtained with K/s_0^2 = (2.2 +/- 0.1) meV/Å^4.

Perhaps the most important structural piece of information about the nanotube sample which can be extracted from the RBM peaks are the (n, m) parameters of the nanotubes. In a nutshell, the assignment of the (n, m) constants can be made by recording spectra with varying excitation energies (and hence probing resonances with various electronic transitions), assuming that ω_{RBM} is proportional to $1/d_t$ and then comparing the resulting resonance peaks to the optical transition energies of tubes with given (n,m) calculated using theoretical models[63,64] (see **Figure 4.8**). Such a procedure also allowed to assign the observed resonance peaks to specific electronic transitions, predicted by these theoretical models[63–65]. Araujo *et al.* also used this method to assign the (n, m) constants and therefore calculate the exact tube diameters to find the RBM frequency/diameter relationship (4.4)[62].

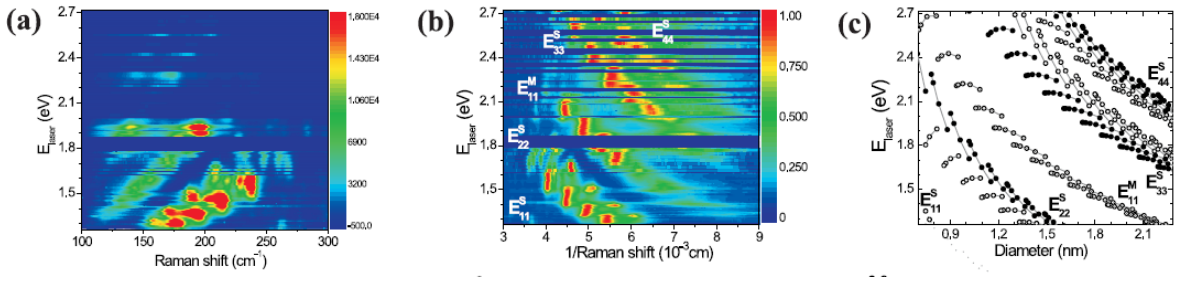

Figure 4.8. (a) 95 Raman spectra of a nanotube sample recorded using various excitation energies. (b) The same spectra plotted as a function of 1/Raman shift, knowing that the RBM frequency is (roughly) inversely proportional to the tube diamter. (c) The theoretical prediction of 5 electronic transition energies for different nanotubes (S – semiconducting, M - metallic); each dot represents one (n,m) nanotube. Taken from[64].

Other research of the nanotube RBM frequencies included changes of RBM in multi-wall nanotubes (MWNT)[66] and weak changes of RBM frequency with chiral angle[67].

4.5. D and D'-bands

The D and D'-bands appear in the Raman spectra of nanocarbons because of disorder which may be present in these materials ("D" stands for "defect" or "disorder")[68]. Just like G'-band, they originate from second-order scattering and they are observed when double resonance occurs. However, D and D'-band come from creation of only one phonon: the excited electron is scattered by a phonon and then is elastically scattered (without loosing energy) from an impurity[68]. **Figure 3.4 b1-b4** shows such processes in graphene for the D'-band. D-band occurs with analogous intervalley resonances. The D and D' bands are also dispersive (their frequencies depend on the exciting laser energy) but the dependence is not as strong as in G' band (for graphite D band around 50 cm^{-1}/eV, D'-band around 10 cm^{-1}/eV compared to G'-band having 100cm^{-1}/eV dependence[68,69]).

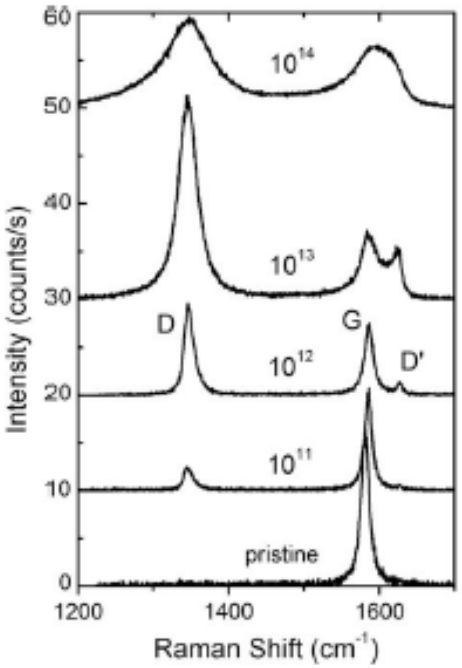

Figure 4.9. Raman spectra of a monolayer graphene sample bombarded with doses 10^{11} – 10^{14} Ar^+/cm^2. Spectra were recorded with nm laser. Taken from[70].

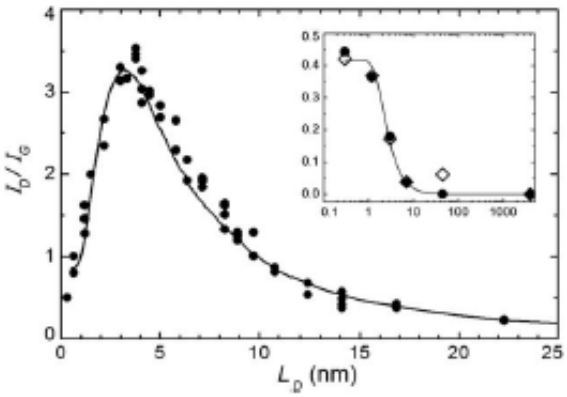

Figure 4.10. The ID/IG ratios for monolayer graphene samples plotted against average distance between defects (LD). Inset shows 50 layer graphene and HOPG (log(LD) on the horizontal axis). From[70].

Graphene. Lucchese *et al.* analyzed Raman spectra of monolayer graphene with point defects resulting from argon ion bombardment[70]. **Figure 4.9** shows the spectra of graphene subjected to different bombardment doses. The ratio of D and G-band intensities (I_D/I_G) plotted as a function of average distance between defects (L_D) is shown in **Figure 4.10**. As can be seen, the plot has a maximum at $L_D \approx 4$ nm. Such behavior was explained by assuming that each ion impact causes changes on two length scales (**Figure 4.11**)[70]. In close proximity (less than r_S, red), the graphene structure becomes disordered while further (between r_S and r_A, green), the structure is preserved but

proximity of the defect causes mixing of certain electronic states and therefore breakdown of selection rules. This way, A-region contributes to the D-band more since in S-region the lattice structure itself is broken. As shown in **Figure 4.11**, gradual bombardment of the graphene sample causes increase of surface areas of both regions (and increase of I_D/I_G) but eventually, the S region dominates and so the I_D/I_G ratio decreases.

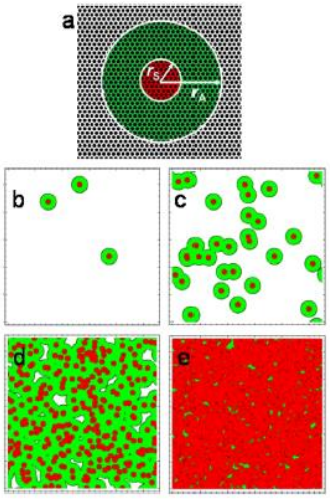

Figure 4.11. Model of point defects in Ar^+-bombarded graphene. From[70].

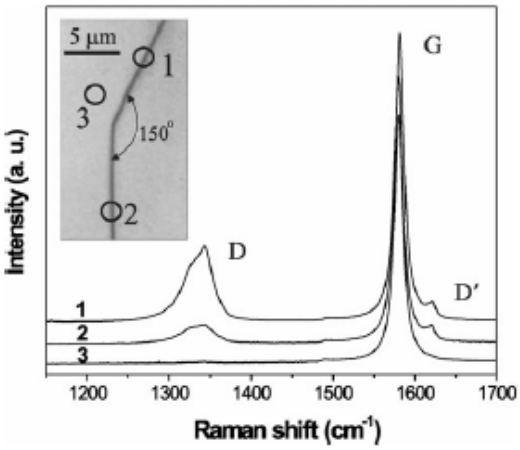

Figure 4.12. Raman spectra of HOPG sample taken in locations 1-3 (photo). Edge 1 has armchair geometry and 2 has zigzag geometry. From[71].

Edges of graphene or graphite can also be considered defects and they give rise to the D-band in the Raman spectrum. Moreover, atomic structure of the edge greatly influences the D-band intensity. **Figure 4.12** shows Raman spectra recorded at the surface and at the edges of a HOPG sample[71]. Scanning tunneling microscopy has shown that edge 1 has armchair geometry while edge 2 has zigzag geometry. As can be seen, the D band is much more intense for the armchair edge. Such result was explained by considering change of electron momentum when it's elastically scattered (see fig.) from the edge[71]. It turned out that during scattering from the zigzag edge no double resonance can occur, and this way a selection rule was derived: D band scattering is forbidden at zigzag edges. Edges of graphene samples obtained by mechanical cleavage of graphite were also analyzed in a similar way[72,73]. However, no obvious D-band intensity dependence on edge geometry was found and the authors attributed it to the roughness of the graphene edges obtained by this method[72]. Finally, in 2010, Krauss *et al.* shown that for pure zigzag graphene edges prepared by carbothermal etching, the D-band indeed disappears[74].

Nanotubes. In case of carbon nanotubes, D-band also increases with increasing degree of disorder, for example when the nanotubes are irradiated[75] or cut to different lengths[76]. However, the D-band of nanotubes is less well understood than in graphene[68].

Near field imaging using D-band wavelength can provide enough spatial resolution to locate a defect along a given nanotube[60]. **Figure 4.12** shows images recorded with wavelengths corresponding to photoluminescence and D-band scattering in a semiconducting SWNT. The site of photoluminescence is the same as the defect location, which suggests that the electron-hole exciton is "trapped" by the defect[60].

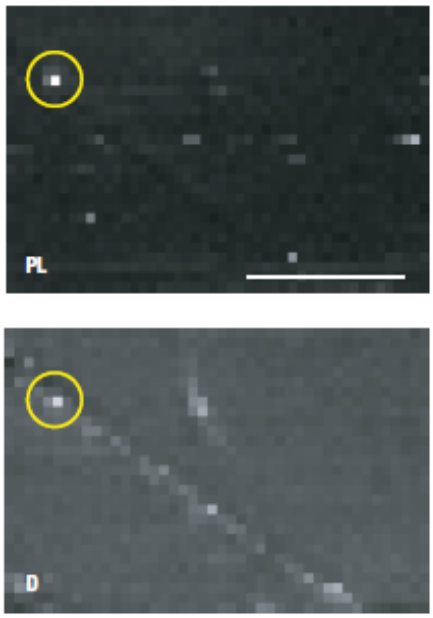

Figure 4.12. Photoluminescence (top) and D-band (bottom) near field images of a (9,1) semiconducting nanotube . From[60].

5. Raman spectroscopy of transition metal dichalcogenides (TMDs)

5.1. TMDs – emerging 2D materials

In the last few years, new two dimensional materials emerged in addition to graphene. One of the most important materials of this type are transition metal dichalcogenides (known as "TMDs" or "TDMCs"). While the phrase "transition metal dichalcogenide" means any chalcogenide of any transition metal, in this context it means a compound with the formula MX_2 where M is the group 4-6 metal and X is a chalcogen (S, Se or Te)[13]. TMDs have a layered structure, where in each layer the plane of metal atoms is between two hexagonal planes of chalcogen atoms, as shown in **Figure 5.1**[13]. These layers are arranged in different structural polytypes, which differ in stacking order and metal coordination (**Figure 5.1 e**).

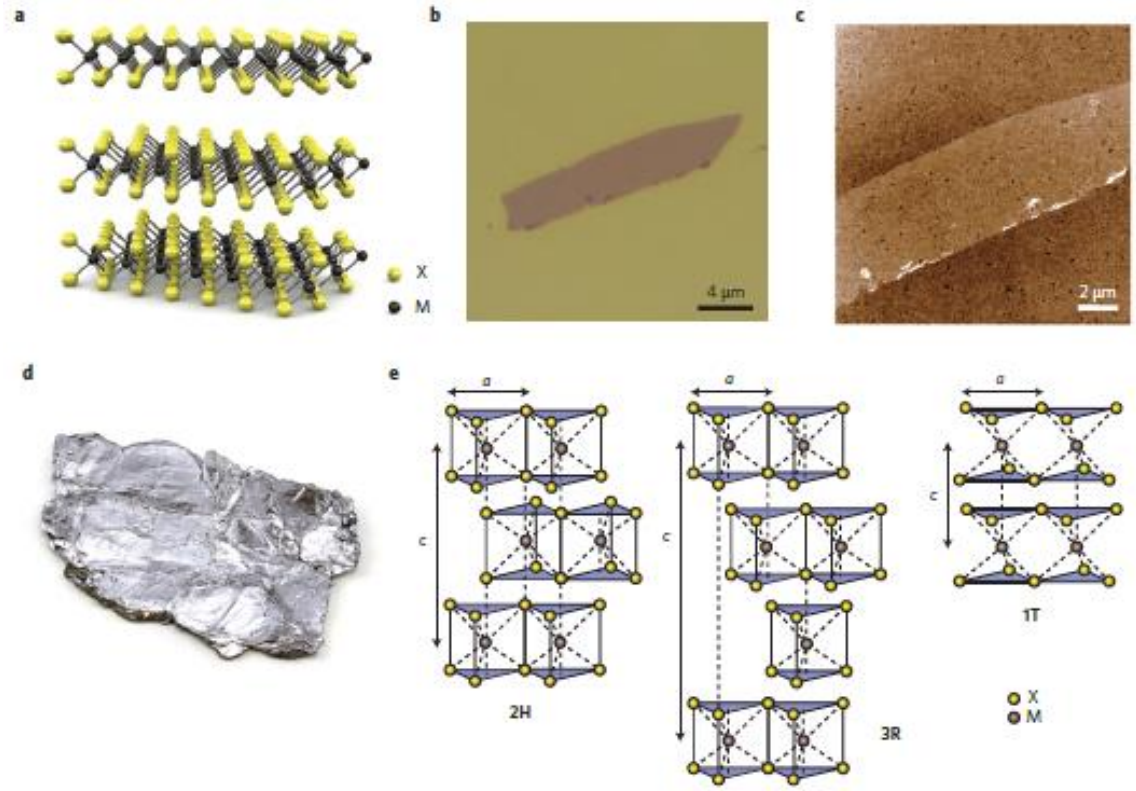

Figure 5.1.. (a) Three dimensional structure of a typical MX_2 TMD, where M are metal and X are chalcogen atoms.(b) Optical microscopy image of a monolayer MoS_2 flake. (c) Atomic force microscopy image of the flake from (b). (d) bulk sample of MoS_2, around 1 cm long. (e) Different polytypes of MX_2: 2H (hexagonal symmetry, two layers per repeat unit, trigonal prismatic coordination), 3R (rhombohedral, three layers per repeat unit, trigonal prismatic coordination) and 1T (tetragonal symmetry, one layer per repeat unit, octahedral coordination). From[13].

Perhaps the most exciting are the electronic and optoelectronic properties of TMDs[13]. Different TMDs can be metallic or semiconducting, with band gaps in the 1 - 2 eV range. The electronic structure of these materials depends on the number of layers: in several TMDs the indirect band gap in the bulk changes to direct band gap in the monolayer. For example, in MoS_2, the bulk indirect band

gap of 1.3 eV changes to 1.8 eV direct band gap when monolayer is obtained[13]. Because of direct band gap, monolayer TMDs are promising materials for optoelectronic applications. This way, TMDs are complementary to graphene, which has zero band gap (it is a semimetal).

Recently (2012 - 2013), two notable reviews were published about TMDs: about electronic and optoelectronic properties, by Wang *et al.*[13] and about their synthesis and chemical properties by Chhowalla *et al*[77].

5.2. Raman spectra – current research

Raman spectra of single- and few-layer TMDs haven't been analyzed as much as spectra of sp^2 nanocarbons, however it's already known that they provide very useful information about given TMD sample

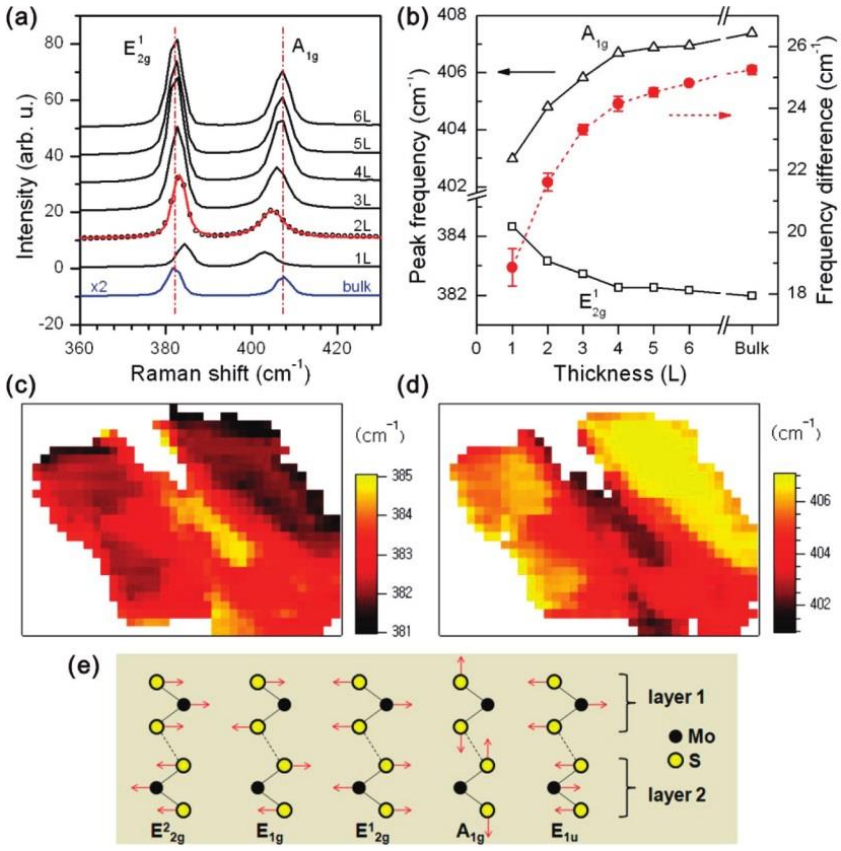

Figure 5.2. (a) Raman spectra of different MoS_2 samples. (b) Variation of the A_{1g} and E^1_{2g} peak frequencies with number of MoS_2 layers. The red line shows the frequency difference. (c) (d) Imaging of a MoS_2 flake using E^1_{2g} and A_{1g} frequencies. (e) 4 Raman-active and 1 IR-active (E1u) vibrational modes in bulk 2H-MoS_2. From[78].

Lee *et al.* performed in 2010 Raman analysis of single- and few-layer MoS_2 flakes on Si/SiO_2 substrate[78]. Out of 4 predicted Raman-active modes for bulk 2H-MoS_2 (**Figure 5.2e**), two bands were observed in the spectra: E^1_{2g} and A_{1g} (**Figure 5.2a**). The absence of the other 2 modes was attributed

to the scattering geometry and to rejection of frequencies near the exciting frequency (Rayleigh-scattered light). It was found that with the decreasing number of layers, the frequency of the E^1_{2g} peak increases while the frequency of the A_{1g} peak decreases. One could expect "softening" of the both modes in the monolayer as the sulfur atoms don't interact with another layer. But surprisingly, the E^1_{2g} mode is "stiffer" in the monolayer. The authors suspected that this may be due to surface reconstruction (it's already known that in bulk MoS_2, the top layer has 5% larger distance between Mo and S planes[79]) and/or interlayer Coulombic interactions[78]. The variation of the E^1_{2g} and A_{1g} peak frequencies allows the identification of the monolayer MoS_2 using Raman spectroscopy. This method has already been used to help confirming that MoS_2 monolayer was obtained[80]. Very similar results were obtained for WS_2 and WSe_2[81].

In 2011, *ab-inito* DFT calculations were performed to find the phonon structure of MoS_2 and WS_2 and to explain the variation of E^1_{2g} and A_{1g} frequencies with the number of layers[82]. The decrease in frequency for the A_{1g} mode was shown to result from interactions between sulfur atoms in adjacent layers, as can be intuitively expected. On the other hand, the unexpected increase of the E^1_{2g} frequency results from increase of the long-range Coulombic interactions associated with decrease of dielectric screening. It was also noted that the change in interatomic distances in a monolayer to the bulk values didn't change the E^1_{2g} frequency much.

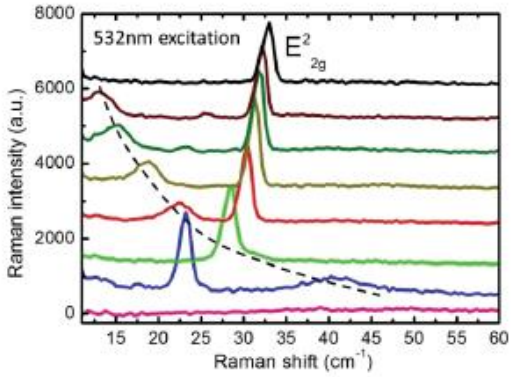

Figure 5.3. Low frequency part of the Raman spectrum of 1-7 layer and bulk MoS2 (bottom to top). The trend line connects the peaks assigned to the compression mode. Adapted from[83].

Besides high energy, A_{1g} and E^1_{2g}, low energy phonons in MoS_2 were also observed by Zeng *et al.* without using resonance excitation frequency, as shown in **Figure 5.3**[83]. The sharp peaks in the spectra at 20 – 35 cm^{-1} were assigned to the E^2_{2g} mode (**Figure 5.2e**). and the broad peaks at 15 – 40 cm^{-1} to the compression mode, which involves displacement of the entire layers in the direction perpendicular to the atom planes. This mode is absent in the bulk as well as monolayer MoS_2. As the position of these two features strongly depend on the number of layers, it was suggested that they can also be used for determination of number of layers in the sample. A detailed study, including

some theoretical (group theory) description about these two modes in 1-19 layer MoS_2 was published by Zhang et al.[84].

Under resonance conditions, many new modes can be identified and the Raman spectra of TMDs become much more complicated. Berkdemir *et al.* analyzed single-layer WS_2 under resonance (514.5 nm laser) and assigned the observed peaks based on *ab-initio* calculations[85]. The most intense peak comes from a double resonance mode 2LA(M) (**Figure 5.4**). In a study by Terrones *et al.*, 1-5 layer and bulk TMD vibration modes were computed and compared to the resonance spectra of the WSe_2, with good agreement[86].

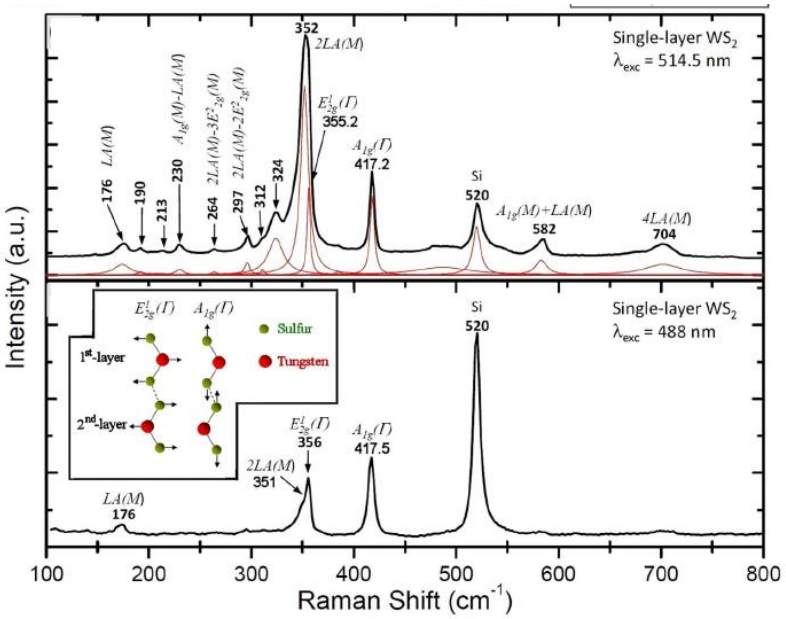

Figure 5.4. Raman spectra of single layer WS2. Top: under resonance conditions. Bottom: outside resonance. Adapted from[85].

In addition to these single and double- resonance features, a triple Raman resonance was observed in monolayer MoS_2[87]. The resonance occurs because of spin-orbit splitting of the electron bands and this observation confirms that such splitting takes place in monolayer MoS_2.

Raman spectroscopy of single and few-layer transition metal dichalcogenides is nowadays a rapidly developing field of research - all of the studies described above were done in the last 4 years. Other recent investigations include: effect of electron doping on monolayer MoS_2 spectra[88], effect of strain[89,90], dependence of spectra on substrates[91,92] and analysis of MoS_2/WS_2 sandwich heterostructures[93]. Knowing how the Raman analysis of nanocarbons developed over the years (see previous sections of this text), one can surely anticipate much more to come.

6. Conclusions

In summary, Raman spectroscopy provides a great deal of information useful to a person investigating carbon nanotubes, graphene and transition metal dichalcogenides. In case of graphene, the spectral features are sensitive to number of layers, stacking order, mechanical strain, presence of defects and geometry of edges. Raman spectra reveal not only structural features but also electronic and phonon structure, allowing experimental verification of theoretical calculations. In nanotube analysis, radial breathing mode allows to find the (n,m) structural indices, making this technique a powerful tool for any nanotube researcher. As for graphene, Raman spectroscopy also allows to probe the predicted theoretical electronic and phonon behavior. Two-dimensional transition metal dichalcogenides, although a young field of study, have already used Raman analysis for similar purposes. Further research in the area of TMD Raman spectroscopy can be expected.

7. References

(1) Raman, C. V; Krishnan, K. S. *Nature* **1928**, *121*, 501.

(2) Miller, F. A.; Kaufhan, G.; Llfe, E. *J. Chem. Educ.* **1989**, *66*, 795.

(3) Fran, A. In *Handbook of Raman Spectroscopy*; Lewis, I. R.; Edwards, H. G. M., Eds.; Marcel Dekker, 2001; pp. 11 – 40.

(4) Nafie, L. A. In *Handbook of Raman Spectroscopy*; Lewis, I. R.; Edwards, H. G. M., Eds.; Marcel Dekker, 2001; pp. 1 – 10.

(5) Ferraro, J. R.; Nakamoto, K. In *Introductory Raman Spectroscopy*; Academic Press, 1994; pp. 160–165.

(6) Baldwin Kurt J; Batchelder, D. N. W. S. In *Handbook of Raman Spectroscopy*; Lewis, I. R.; Edwards, H. G. M., Eds.; Marcel Dekker, 2001; pp. 145 – 190.

(7) Treado Patrick J; Nelson, M. P. In *Handbook of Raman Spectroscopy*; Lewis, I. R.; Edwards, H. G. M., Eds.; Marcel Dekker, 2001; pp. 191 – 250.

(8) Ferraro, J. R.; Nakamoto, K. In *Introductory Raman Spectroscopy*; Academic Press, 1994; pp. 142 – 147.

(9) Edwards, H. G. M. In *Handbook of Raman Spectroscopy*; Lewis, I. R.; Edwards, H. G. M., Eds.; Marcel Dekker, 2001; pp. 1011 – 1044.

(10) Lewis, I. R. In *Handbook of Raman Spectroscopy*; Lewis, I. R.; Edwards, H. G. M., Eds.; Marcel Dekker, 2001; pp. 919 – 974.

(11) Dresselhaus, M. S.; Dresselhaus, G.; Saito, R.; Jorio, a. *Phys. Rep.* **2005**, *409*, 47.

(12) Malard, L. M.; Pimenta, M. a.; Dresselhaus, G.; Dresselhaus, M. S. *Phys. Rep.* **2009**, *473*, 51.

(13) Wang, Q. H.; Kalantar-Zadeh, K.; Kis, A.; Coleman, J. N.; Strano, M. S. *Nat. Nanotechnol.* **2012**, *7*, 699.

(14) Jayaraman, A.; Ramdas, A. K. *Phys. Today* **1988**, *41*, 56.

(15) Raman, C. V. *Philos. Mag. Ser. 6* **1906**, *12*, 494.

(16) Raman, C. V. *Philos. Mag. Ser. 6* **1907**, *14*, 591.

(17) Raman, C. V. *Nature* **1921**, *108*, 367.

(18) Raman, C. V; Krishnan, K. S. *Nature* **1928**, *121*, 711.

(19) The Nobel Prize in Physics 1930 http://www.nobelprize.org/nobel_prizes/physics/laureates/1930/ (accessed May 14, 2014).

(20) Ferraro, J. R.; Nakamoto, K.; Brown, C. W. In *Introductory Raman Spectroscopy*; Academic Press, 2003; pp. 13–17.

(21) Jorio, A.; Dresselhaus, M. S.; Saito, R.; Dresselhaus, G. In *Raman Spectroscopy in Graphene Related Systems*; Wiley-VCH, 2011; pp. 73–78.

(22) Koningstein, J. A. In *Introduction to the Theory of Raman Effect*; D. Reidel: Dordrecht, 1972; pp. 84 – 91.

(23) Jorio, A.; Dresselhaus, M. S.; Saito, R.; Dresselhaus, G. In *Raman Spectroscopy in Graphene Related Systems*; Wiley-VCH, 2011; pp. 78–87.

(24) Jorio, A.; Dresselhaus, M. S.; Saito, R.; Dresselhaus, G. F. In *Raman Spectroscopy in Graphene Related Systems*; Wiley-VCH, 2011; pp. 73 – 101.

(25) Jorio, A.; Souza Filho, A. G.; Dresselhaus, G.; Dresselhaus, M. S.; Saito, R.; Hafner, J. H.; Lieber, C. M.; Matinaga, F. M.; Dantas, M. S. S.; Pimenta, M. A. *Phys. Rev. B* **2001**, *63*, 245416.

(26) Souza Filho, A. G.; Jorio, A.; Hafner, J. H.; Lieber, C. M.; Saito, R.; Pimenta, M. A.; Dresselhaus, G.; Dresselhaus, M. S. *Phys. Rev. B* **2001**, *63*, 241404.

(27) Jorio, A.; Dresselhaus, M. S.; Saito, R.; Dresselhaus, G. F. In *Raman Spectroscopy in Graphene Related Systems*; Wiley-VCH, 2011; pp. 103–116.

(28) Pimenta, M. A.; Dresselhaus, G.; Dresselhaus, M. S.; Cancado, L. G.; Jorio, A.; Saito, R. *Phys. Chem. Chem. Phys.* **2007**, *9*, 1276.

(29) Ferraro, J. R.; Nakamoto, K. In *Introductory Raman Spectroscopy*; Academic Press, 2003; pp. 1 – 94.

(30) Jorio, A.; Dresselhaus, M. S.; Saito, R.; Dresselhaus, G. F. In *Raman Spectroscopy in Graphene Related Systems*; Wiley-VCH, 2011; pp. 121 – 153.

(31) Koningstein, J. A. *Introduction to the Theory of the Raman Effect*; D. Reidel, 1972.

(32) Kroto, H. W.; Heath, J. R.; O'Brien, S. C.; Curl, R. F.; Smalley, R. E. *Nature* **1985**, *318*, 162.

(33) Iijima, S. *Nature* **1991**, *354*, 56.

(34) Iijima, S.; Ichihashi, T. *Nature* **1993**, *363*, 603.

(35) Bethune, D. S.; Klang, C. H.; de Vries, M. S.; Gorman, G.; Savoy, R.; Vazquez, J.; Beyers, R. *Nature* **1993**, *363*, 605.

(36) *Carbon Nanotubes: Advanced Topics in the Synthesis, Structure, Properties and Applications*; Jorio, A.; Dresselhaus, G.; Dresselhaus, M. S., Eds.; Springer, 2008.

(37) Harris, P. J. F. *Carbon Nanotube Science: Synthesis, Properties and Applications*; 2nd ed.; Cambridge University Press, 2011.

(38) Pugno, N. M. *J. Phys. Condens. Matter* **2006**, *18*, S1971.

(39) Novoselov, K. S.; Geim, A. K.; Morozov, S. V; Jiang, D.; Zhang, Y.; Dubonos, S. V; Grigorieva, I. V; Firsov, a a. *Science* **2004**, *306*, 666.

(40) Geim, A. K.; Novoselov, K. S. *Nat Mater* **2007**, *6*, 183.

(41) Castro Neto, A. H.; Guinea, F.; Peres, N. M. R.; Novoselov, K. S.; Geim, A. K. *Rev. Mod. Phys.* **2009**, *81*, 109.

(42) Dresselhaus, M. S.; Jorio, A.; Hofmann, M.; Dresselhaus, G.; Saito, R. *Nano Lett.* **2010**, *10*, 751.

(43) Jorio, A.; Dresselhaus, M. S.; Saito, R.; Dresselhaus, G. F. *Raman Spectroscopy in Graphene Related Systems*; Wiley-VCH, 2011.

(44) Jorio, A.; Dresselhaus, M. S.; Saito, R.; Dresselhaus, G. F. In *Raman Spectroscopy in Graphene Related Systems*; Wiley-VCH, 2011; pp. 88 – 98.

(45) Jorio, A.; Dresselhaus, M. S.; Saito, R.; Dresselhaus, G. F. In *Raman Spectroscopy in Graphene Related Systems*; WILEY-VCH, 2011; pp. 161 – 177.

(46) Mohiuddin, T. M. G.; Lombardo, A.; Nair, R. R.; Bonetti, A.; Savini, G.; Jalil, R.; Bonini, N.; Basko, D. M.; Galiotis, C.; Marzari, N.; Novoselov, K. S.; Geim, A. K.; Ferrari, A. C. *Phys. Rev. B* **2009**, *79*, 205433.

(47) Reich, S.; Thomsen, C.; Ordejón, P. *Phys. Rev. B* **2001**, *64*, 195416.

(48) Jorio, A.; Pimenta, M. A.; Souza Filho, A. G.; Samsonidze, G. G.; Swan, A. K.; Ünlü, M. S.; Goldberg, B. B.; Saito, R.; Dresselhaus, G.; Dresselhaus, M. S. *Phys. Rev. Lett.* **2003**, *90*, 107403.

(49) Jorio, A.; Souza Filho, A. G.; Dresselhaus, G.; Dresselhaus, M. S.; Swan, A. K.; Ünlü, M. S.; Goldberg, B. B.; Pimenta, M. A.; Hafner, J. H.; Lieber, C. M.; Saito, R. *Phys. Rev. B* **2002**, *65*, 155412.

(50) Pimenta, M. A.; Marucci, A.; Empedocles, S. A.; Bawendi, M. G.; Hanlon, E. B.; Rao, A. M.; Eklund, P. C.; Smalley, R. E.; Dresselhaus, G.; Dresselhaus, M. S. *Phys. Rev. B* **1998**, *58*, R16016.

(51) Dubay, O.; Kresse, G.; Kuzmany, H. *Phys. Rev. Lett.* **2002**, *88*, 235506.

(52) Jorio, A.; Dresselhaus, M. S.; Saito, R.; Dresselhaus, G. F. In *Raman Spectroscopy in Graphene Related Systems*; Wiley-VCH, 2011; pp. 277 – 298.

(53) Mafra, D. L.; Samsonidze, G.; Malard, L. M.; Elias, D. C.; Brant, J. C.; Plentz, F.; Alves, E. S.; Pimenta, M. A. *Phys. Rev. B* **2007**, *76*, 233407.

(54) Ferrari, A. C.; Meyer, J. C.; Scardaci, V.; Casiraghi, C.; Lazzeri, M.; Mauri, F.; Piscanec, S.; Jiang, D.; Novoselov, K. S.; Roth, S.; Geim, A. K. *Phys. Rev. Lett.* **2006**, *97*, 187401.

(55) Malard, L. M.; Nilsson, J.; Elias, D. C.; Brant, J. C.; Plentz, F.; Alves, E. S.; Castro Neto, A. H.; Pimenta, M. A. *Phys. Rev. B* **2007**, *76*, 201401.

(56) Cançado, L. G.; Reina, A.; Kong, J.; Dresselhaus, M. S. *Phys. Rev. B* **2008**, *77*, 245408.

(57) Poncharal, P.; Ayari, A.; Michel, T.; Sauvajol, J.-L. *Phys. Rev. B* **2008**, *78*, 113407.

(58) Souza Filho, A. G.; Jorio, A.; Dresselhaus, G.; Dresselhaus, M. S.; Saito, R.; Swan, A. K.; Ünlü, M. S.; Goldberg, B. B.; Hafner, J. H.; Lieber, C. M.; Pimenta, M. A. *Phys. Rev. B* **2001**, *65*, 35404.

(59) Souza Filho, A. G.; Jorio, A.; Swan, A. K.; Ünlü, M. S.; Goldberg, B. B.; Saito, R.; Hafner, J. H.; Lieber, C. M.; Pimenta, M. A.; Dresselhaus, G.; Dresselhaus, M. S. *Phys. Rev. B* **2002**, *65*, 85417.

(60) Maciel, I. O.; Anderson, N.; Pimenta, M. A.; Hartschuh, A.; Qian, H.; Terrones, M.; Terrones, H.; Campos-Delgado, J.; Rao, A. M.; Novotny, L.; Jorio, A. *Nat Mater* **2008**, *7*, 878.

(61) Jorio, A.; Dresselhaus, M. S.; Saito, R.; Dresselhaus, G. F. In *Raman Spectroscopy in Graphene Related Systems*; Wiley-VCH, 2011; pp. 199 – 222.

(62) Araujo, P. T.; Maciel, I. O.; Pesce, P. B. C.; Pimenta, M. A.; Doorn, S. K.; Qian, H.; Hartschuh, A.; Steiner, M.; Grigorian, L.; Hata, K.; Jorio, A. *Phys. Rev. B* **2008**, *77*, 241403.

(63) Fantini, C.; Jorio, A.; Souza, M.; Strano, M. S.; Dresselhaus, M. S.; Pimenta, M. A. *Phys. Rev. Lett.* **2004**, *93*, 147406.

(64) Araujo, P. T.; Doorn, S. K.; Kilina, S.; Tretiak, S.; Einarsson, E.; Maruyama, S.; Chacham, H.; Pimenta, M. A.; Jorio, A. *Phys. Rev. Lett.* **2007**, *98*, 67401.

(65) Araujo, P. T.; Jorio, A. *Phys. status solidi* **2008**, *245*, 2201.

(66) Villalpando-Paez, F.; Muramatsu, H.; Kim, Y. A.; Farhat, H.; Endo, M.; Terrones, M.; Dresselhaus, M. S. *Nanoscale* **2010**, *2*, 406.

(67) Jorio, A.; Fantini, C.; Pimenta, M. A.; Capaz, R. B.; Samsonidze, G. G.; Dresselhaus, G.; Dresselhaus, M. S.; Jiang, J.; Kobayashi, N.; Grüneis, A.; Saito, R. *Phys. Rev. B* **2005**, *71*, 75401.

(68) Jorio, A.; Dresselhaus, M. S.; Saito, R.; Dresselhaus, G. F. In *Raman Spectroscopy in Graphene Related Systems*; Wiley-VCH, 2011; pp. 299 – 323.

(69) Vidano, R. P.; Fischbach, D. B.; Willis, L. J.; Loehr, T. M. *Solid State Commun.* **1981**, *39*, 341.

(70) Lucchese, M. M.; Stavale, F.; Ferreira, E. H. M.; Vilani, C.; Moutinho, M. V. O.; Capaz, R. B.; Achete, C. A.; Jorio, A. *Carbon N. Y.* **2010**, *48*, 1592.

(71) Cançado, L. G.; Pimenta, M. A.; Neves, B. R. A.; Dantas, M. S. S.; Jorio, A. *Phys. Rev. Lett.* **2004**, *93*, 247401.

(72) Gupta, A. K.; Russin, T. J.; Gutiérrez, H. R.; Eklund, P. C. *ACS Nano* **2008**, *3*, 45.

(73) Casiraghi, C.; Hartschuh, A.; Qian, H.; Piscanec, S.; Georgi, C.; Fasoli, A.; Novoselov, K. S.; Basko, D. M.; Ferrari, A. C. *Nano Lett.* **2009**, *9*, 1433.

(74) Krauss, B.; Nemes-Incze, P.; Skakalova, V.; Biro, L. P.; Klitzing, K. von; Smet, J. H. *Nano Lett.* **2010**, *10*, 4544.

(75) Hulman, M.; Skákalová, V.; Roth, S.; Kuzmany, H. *J. Appl. Phys.* **2005**, *98*, 024311.

(76) Chou, S. G.; Son, H.; Kong, J.; Jorio, A.; Saito, R.; Zheng, M.; Dresselhaus, G.; Dresselhaus, M. S. *Appl. Phys. Lett.* **2007**, *90*.

(77) Chhowalla, M.; Shin, H. S.; Eda, G.; Li, L.-J.; Loh, K. P.; Zhang, H. *Nat. Chem.* **2013**, *5*, 263.

(78) Lee, C.; Yan, H.; Brus, L. E.; Heinz, T. F.; Hone, J.; Ryu, S. *ACS Nano* **2010**, *4*, 2695.

(79) Mrstik, B. J.; Kaplan, R.; Reinecke, T. L.; Van Hove, M.; Tong, S. Y. *Phys. Rev. B* **1977**, *15*, 897.

(80) Sundaram, R. S.; Engel, M.; Lombardo, A.; Krupke, R.; Ferrari, a C.; Avouris, P.; Steiner, M. *Nano Lett.* **2013**, *13*, 1416.

(81) Zhao, W.; Ghorannevis, Z.; Amara, K. K.; Pang, J. R.; Toh, M.; Zhang, X.; Kloc, C.; Tan, P. H.; Eda, G. *Nanoscale* **2013**, *5*, 9677.

(82) Molina-Sánchez, A.; Wirtz, L. *Phys. Rev. B* **2011**, *84*, 155413.

(83) Zeng, H.; Zhu, B.; Liu, K.; Fan, J.; Cui, X.; Zhang, Q. M. *Phys. Rev. B* **2012**, *86*, 241301.

(84) Zhang, X.; Han, W. P.; Wu, J. B.; Milana, S.; Lu, Y.; Li, Q. Q.; Ferrari, A. C.; Tan, P. H. *Phys. Rev. B* **2013**, *87*, 115413.

(85) Berkdemir, A.; Gutierrez, H. R.; Botello-Mendez, A. R.; Perea-Lopez, N.; Elias, A. L.; Chia, C.-I.; Wang, B.; Crespi, V. H.; Lopez-Urias, F.; Charlier, J.-C.; Terrones, H.; Terrones, M. *Sci. Rep.* **2013**, *3*.

(86) Terrones, H.; Corro, E. Del; Feng, S.; Poumirol, J. M.; Rhodes, D.; Smirnov, D.; Pradhan, N. R.; Lin, Z.; Nguyen, M. A. T.; Elias, A. L.; Mallouk, T. E.; Balicas, L.; Pimenta, M. A.; Terrones, M. *Sci. Rep.* **2014**, *4*.

(87) Sun, L.; Yan, J.; Zhan, D.; Liu, L.; Hu, H.; Li, H.; Tay, B. K.; Kuo, J.-L.; Huang, C.-C.; Hewak, D. W.; Lee, P. S.; Shen, Z. X. *Phys. Rev. Lett.* **2013**, *111*, 126801.

(88) Chakraborty, B.; Bera, A.; Muthu, D. V. S.; Bhowmick, S.; Waghmare, U. V; Sood, A. K. *Phys. Rev. B* **2012**, *85*, 161403.

(89) Wang, Y.; Cong, C.; Qiu, C.; Yu, T. *Small* **2013**, *9*, 2857.

(90) Rice, C.; Young, R. J.; Zan, R.; Bangert, U.; Wolverson, D.; Georgiou, T.; Jalil, R.; Novoselov, K. S. *Phys. Rev. B* **2013**, *87*, 81307.

(91) Su, L.; Zhang, Y.; Yu, Y.; Cao, L. *Nanoscale* **2014**, *6*, 4920.

(92) Buscema, M.; Steele, G.; van der Zant, H. J.; Castellanos-Gomez, A. *Nano Res.* **2014**, *7*, 1.

(93) Liang, L.; Meunier, V. *Nanoscale* **2014**, *6*, 5394.

(94) Jorio, A.; Pimenta, M. A.; Filho, A. G. S.; Saito, R.; Dresselhaus, G.; Dresselhaus, M. S. *New J. Phys.* **2003**, *5*, 139.